APPLIED PHYSICS

Topological mechanics of knots and tangles

Vishal P. Patil[1], Joseph D. Sandt[2], Mathias Kolle[2], Jörn Dunkel[1]*

Knots play a fundamental role in the dynamics of biological and physical systems, from DNA to turbulent plasmas, as well as in climbing, weaving, sailing, and surgery. Despite having been studied for centuries, the subtle interplay between topology and mechanics in elastic knots remains poorly understood. Here, we combined optomechanical experiments with theory and simulations to analyze knotted fibers that change their color under mechanical deformations. Exploiting an analogy with long-range ferromagnetic spin systems, we identified simple topological counting rules to predict the relative mechanical stability of knots and tangles, in agreement with simulations and experiments for commonly used climbing and sailing bends. Our results highlight the importance of twist and writhe in unknotting processes, providing guidance for the control of systems with complex entanglements.

Knots are among the oldest, most enduring human technologies, as valuable to ancient builders (*1*) and mariners (*2*) as to modern engineers and surgeons (*3*). Thought to predate the wheel (*1*), knotted structures owe their extraordinary longevity and widespread usage to an inherent mechanical robustness that arises from the subtle interplay of topology, elasticity, and friction. Over the course of many centuries, sailors, weavers, climbers, and surgeons have acquired a wealth of knowledge about the benefits and drawbacks of various types of knots (*1*, *2*). Experience has taught us that certain knots are more stable than others, but we are still largely unable to predict the mechanical behavior of knots and tangles from basic topological observables (*4*), such as the number and relative ordering of crossings. Although recent experimental and theoretical research has revealed important insights into the competition between force transmission and friction in special classes of knots (*5*, *6*), hitches (*7*), and fabrics (*8*), there currently exists no comprehensive mathematical theory (*9*) linking the topological and mechanical properties of knotted elastic structures.

Physical knots and their topology first assumed a central role in science with the introduction of Kelvin's vortex-atom model in the 1860s (*10*). Since then, the fundamental importance of entangled structures has become firmly established in a diverse range of disciplines and contexts (*9*). In physics, for example, interactions between knotted defect lines are essential to understanding and controlling dynamics and mixing in classical and complex fluids (*11*–*14*), including liquid crystals (*15*), plasmas (*16*), and quantum fluids (*17*). Whereas the energetic costs associated with topological transformations are typically low in liquids and gases (*17*), they tend to become prohibitively large in entangled solids (*5*, *6*). This fact has profound consequences for the stability and function of natural and engineered structures, from the microscopic knots in DNA (*18*, *19*), proteins (*20*–*22*), and polymers (*23*) to knitted clothes (*8*) and macroscopic meshworks (*24*). Achieving a unified understanding of these various systems requires taking into account not only their topological but also their elastic properties. Because key concepts from topology and elasticity theory remain applicable over a wide range of scales, deciphering the topological principles (*5*, *6*, *9*) that determine the mechanical stability of knots promises insights into a broad spectrum of physically entangled structures. Therefore, our main goal is to identify generic topological counting rules that enable us to estimate which members of a given family of elastic knots are the most robust against untying. To this end, we combined elements from mathematical and physical knot theory (*9*, *25*) with optomechanical experiments and quantitative continuum modeling (Fig. 1).

We were interested in tying two lines together so that they form a stable longer rope, a task known as "tying a bend" among sailors (*2*). Mathematically, this configuration describes an oriented 2-tangle, defined as the union of two oriented open curves embedded in space (*4*). Although an elegant mathematical formalism exists to describe certain simple families of 2-tangles (*26*), little is known theoretically about even the most basic bend knots used in practice. We constructed a topological phase diagram that explains the relative stability of a selection of bends that are commonly used in the sailing and climbing communities. To validate the underlying topological model, we compared its predictions with simulations of an optomechanically verified continuum theory and with quantitative measurements using laboratory "prisoner's escape" experiments.

Our optomechanical experiments use recently developed color-changing photonic fibers (*27*) that allow for the imaging of strain in knots (Fig. 1, A and B). These fibers derive structural color from a multilayer cladding composed of alternating layers of transparent elastomers with distinct refractive indices wrapped around an elastic core. Their coloration varies with the thickness of layers in the periodic cladding, which changes upon elongation or bending. As is typical of macroscopic materials at room temperature, the persistence lengths of the fibers used in our experiments are several orders of magnitude larger than the diameters of the tightened knots (*28*), with empirical knowledge (*2*) indicating that essential knot properties are only weakly dependent on the elastic modulus. Theoretically, we describe knotted fibers using a damped Kirchhoff model (*5*, *28*, *29*) validated through comparison with photographs depicting the strain-induced color changes in mechanoresponsive photonic fibers (Fig. 1, A to C). Simulating the tightening process of a 1-tangle, corresponding to a single knotted fiber pulled at both ends (Fig. 1, A and B, and movie S1), reveals the relative strengths and localization of the bending and stretching strains (Fig. 1, D and E), which are not individually discernible in our experiments. Furthermore, the Kirchhoff model highlights why topological considerations (*4*) alone do not suffice to explain the mechanical behaviors (*2*) of real-world knots: Loosening or tightening a knot transforms any of its planar projections according to a sequence of three elementary topology-preserving Reidemeister moves, R_1, R_2, and R_3 (Fig. 1F). Despite being topologically equivalent, the move R_1 is energetically distinct as it involves substantial changes in strain, whereas moves R_2 and R_3 are energetically favored soft modes (Fig. 1F), implying that physical knots preferentially deform by R_2 and R_3. Thus, to link the physical properties of tangled fibers to their topology, one must merge concepts from classical mathematical knot theory (*4*) with elasticity theory (*5*, *6*, *9*, *30*).

Continuum simulations provide guidance for how one can complement bare topological knot diagrams (*4*) with coarse-grained mechanical information that is essential for explaining why certain knots are more stable than others (Fig. 2). In contrast to a 1-tangle, which is tightened by pulling diametrically at its two ends (Fig. 2A), each strand of a bend knot has one pulled and one free end (Fig. 2B). Therefore, the local fiber velocity directions in the center-of-mass frame of the bend knot define natural fiber orientations on the underlying 2-tangle (Fig. 2B), thus establishing mapping between bends and oriented 2-tangles. At each contact crossing, the fibers mutually generate a frictional self-torque with well-defined handedness, depending on the relative velocity and ordering of the two fiber strands (Fig. 2, B

[1]Department of Mathematics, Massachusetts Institute of Technology, Cambridge, MA 02139, USA. [2]Department of Mechanical Engineering, Massachusetts Institute of Technology, Cambridge, MA 02139, USA.
*Corresponding author. Email: dunkel@mit.edu

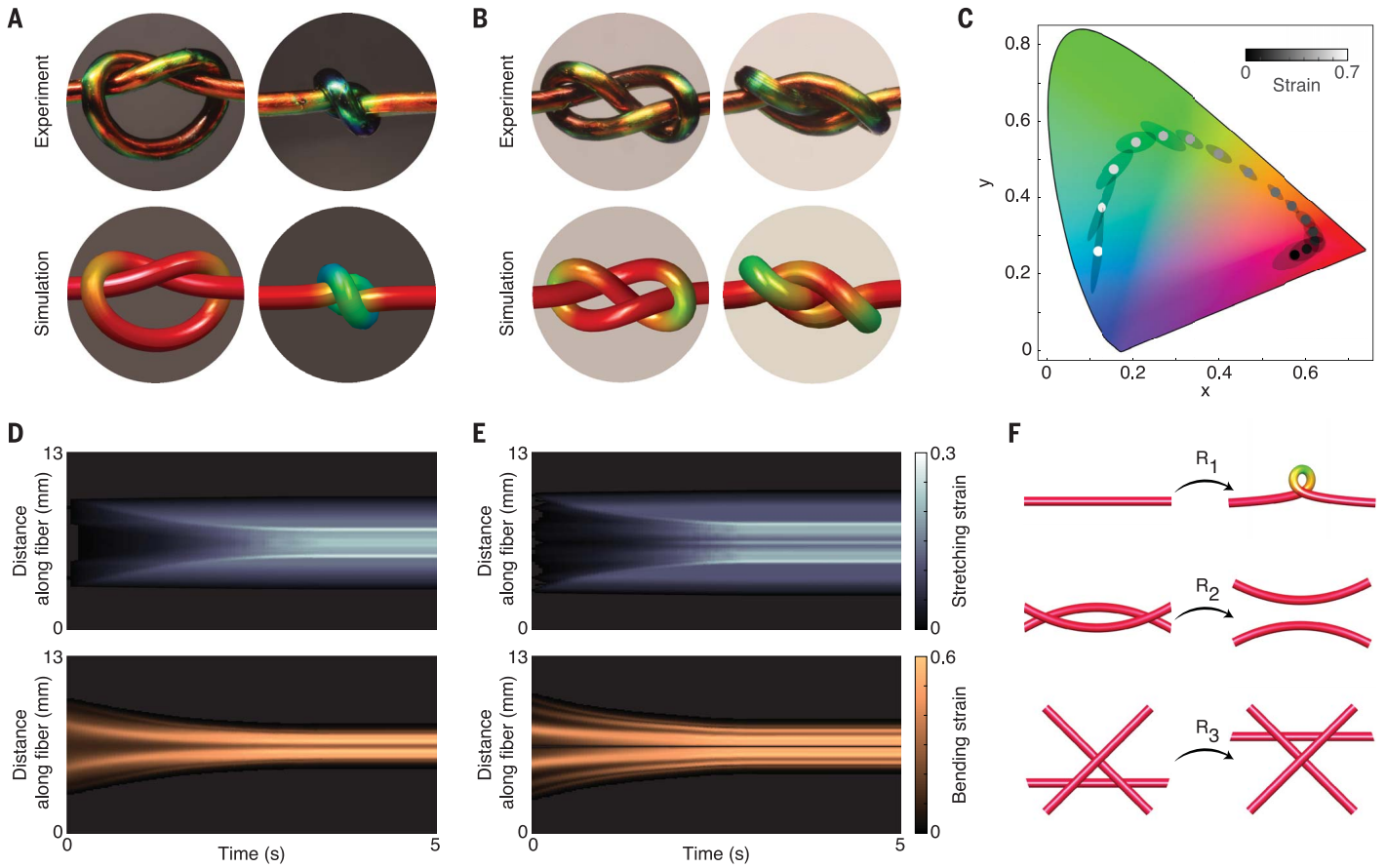

Fig. 1. Experiments and simulations reveal mechanical properties of knots. (**A** and **B**) Color-changing mechanoresponsive fibers confirm the stress patterns predicted by continuum simulations for the trefoil knot (A) and the figure-of-eight knot (B) during the tightening process (movie S1). Fiber diameter is 0.4 mm. (**C**) Dependence of fiber color on strain visualized as a trajectory in the CIE 1931 XYZ color space, where mean positions (solid circles) lie within standard deviation ellipses (*28*). This strain color coding is used in panels (A), (B), and (F). (**D** and **E**) Simulations revealing the relative strength of bending and stretching strains along knots. (D) and (E) show the evolution of these two complementary strain contributions during tightening of the trefoil knot in (A) and the figure-of-eight knot in (B). Pulling force is 0.02 N. The elastic moduli are given in (*28*). (**F**) Topology-preserving Reidemeister moves affect the elastic energy of the underlying fibers differently. Move R_1 induces strain and thus requires higher energy than R_2 and R_3, highlighting that both topological and elastic properties determine the mechanical behavior of knots.

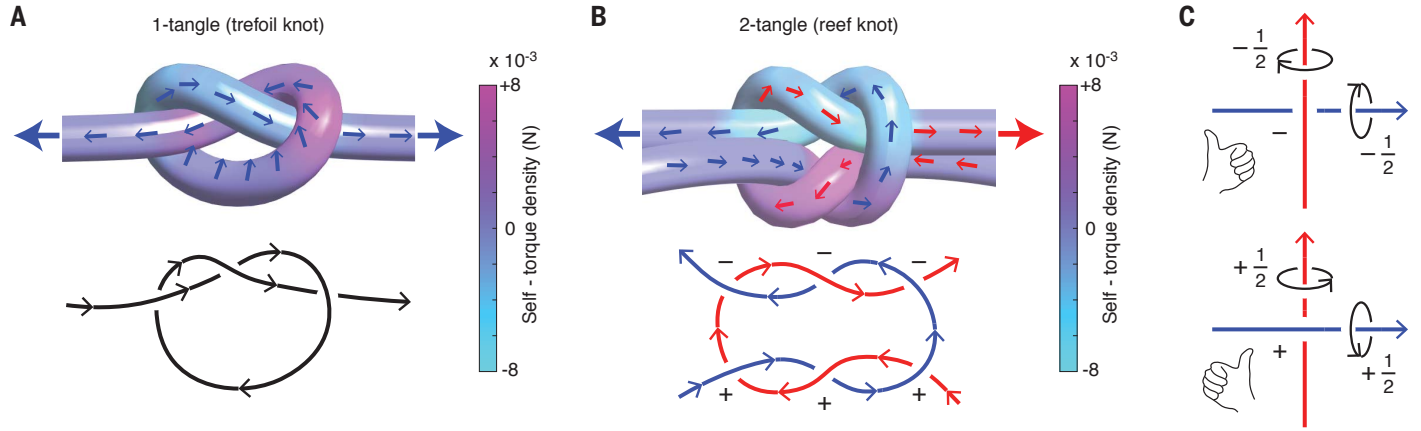

Fig. 2. Topology and self-twisting in 1-tangles and 2-tangles. (**A**) Top: A 1-tangle is tightened by pulling its two ends in opposite directions (large exterior arrows). The induced fiber velocity field (small interior arrows) in the center-of-mass frame reverses its orientation near the fiber midpoint. Bottom: As the velocity field is incompatible with any chosen global fiber orientation (black arrows), self-torque data cannot be consistently assigned to a topological 1-tangle diagram. (**B**) Top: Because of the presence of the two free ends, the pulling directions of a bend knot (large exterior arrows) define a canonical global orientation on each of the two fibers in the corresponding 2-tangle. Bottom: The alignment of local velocity directions and fiber orientation permits the discretization of self-torque data over crossings by assigning twist charges $q_i = \pm 1$ to each vertex i as described in the next panel. (**C**) Each individual fiber strand passing through vertex i induces a rotation in the other strand, thus contributing ±1/2 to the vertex twist charge $q_i = \pm 1$, with sign corresponding to rotation handedness. Blue–blue and red–red self-crossings found in more complex 2-tangles can be labeled accordingly. The sum of the q_i defines the total writhe Wr, providing a coarse-grained approximation of the total self-torque in 2-tangles; the reef knot has $Wr = 0$. Fiber diameter is 0.4 mm and pulling force is 15 N in (A) and (B).

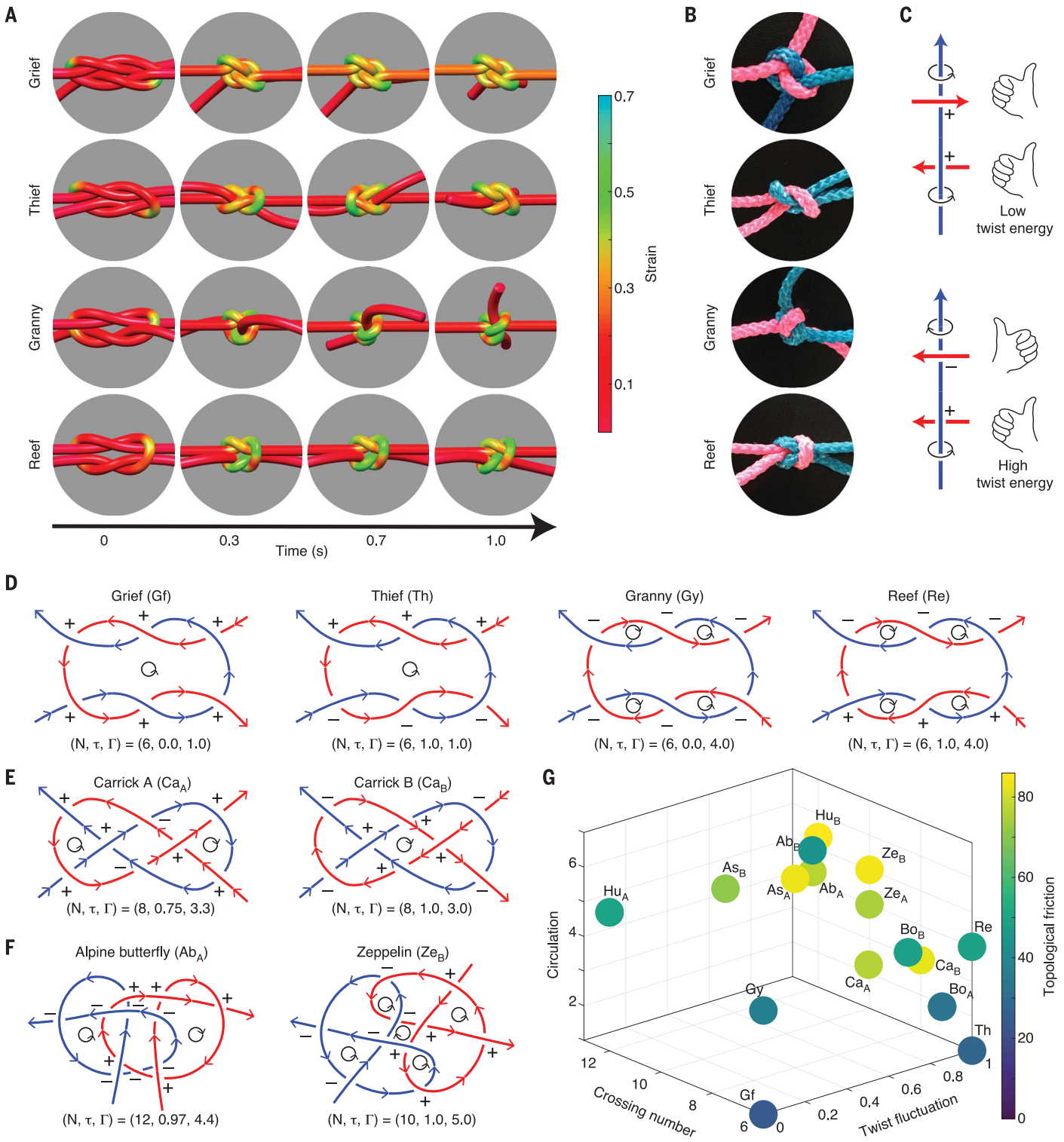

Fig. 3. Topology determines the mechanical stability of 2-tangles. (**A**) Small modifications in topology lead to substantial changes in the mechanical behavior of 2-tangles, exemplified by the presence or absence of global rotation of the knot body upon pulling (movie S2); fiber diameter is 0.4 mm and pulling force is 15 N. Knots are shown in order of least stable (grief knot) to most stable (reef knot). (**B**) Simulated tight configurations of knots are validated with real knots tied in nylon rope (diameter, 20 mm) with horizontal ends being pulled. (**C**) Tight knots act on themselves by right-handed (positive) and left-handed (negative) torques. Equally directed torques lead to rolling (top), whereas opposite torques promote locking (bottom) and thus stabilize a knot against untying. (**D** to **F**) Knot diagrams oriented by pulling direction correspond to a topological state defined as the triple of crossing number N, twist fluctuation τ, and circulation Γ. These parameters explain the relative stability of knots in the reef group (D) and the Carrick group (E). (F) The Zeppelin bend is more stable than the alpine butterfly bend, displaying both higher twist fluctuation and higher circulation. (**G**) Topological state reveals the underlying structure of bend knots and separates stable knots from unstable knots. The dimensionless topological friction, obtained from simulation, is determined by the velocity response when the knot is pulled with a given force and is a measure of the friction force caused by the knot (*28*). Labels in (G) correspond to those in (D), (E), and (F) and additional knots listed in fig. S3.

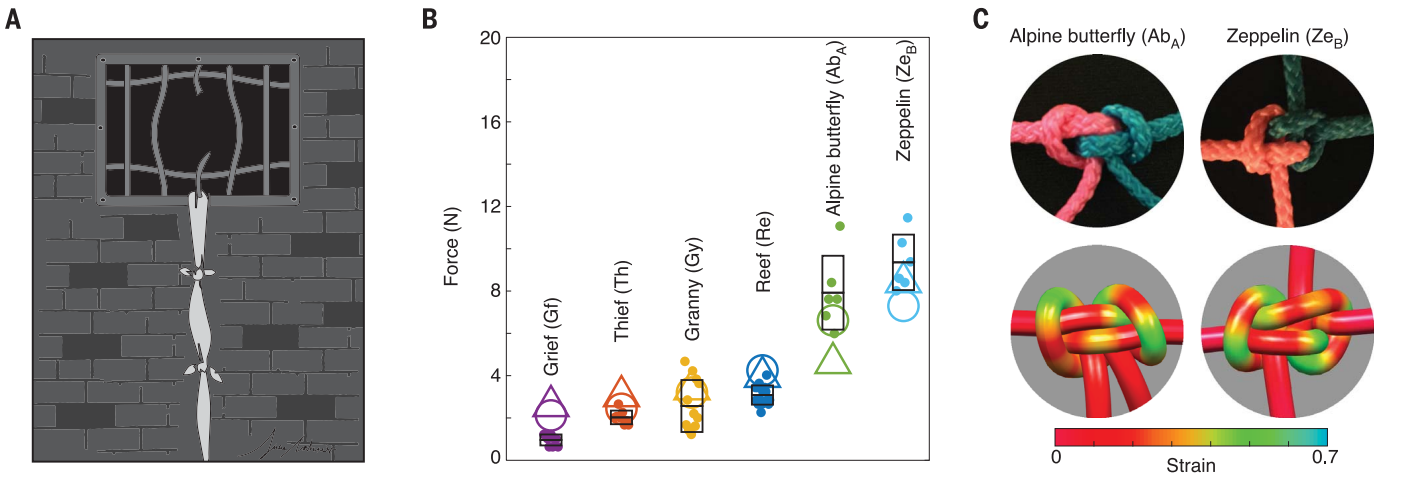

Fig. 4. Experiments for commonly used knots validate the theoretically predicted phase diagram. (**A**) Our experimental setup (*28*) mimics the classical prisoner's escape problem by determining the critical pulling force $F = mg$ at which two lines untie. (**B**) Experiments measuring the critical mass m at which two Dyneema fibers untie confirm the ranking of knot stability predicted by simulations. For simpler knots with crossing number ≤8, averages (horizontal lines) over individual experiments (small filled circles) agree quantitatively with the relative strength predicted from simulations measuring both the velocity-based friction (large empty circles) and the total compression force (large empty triangles) within the knot (*28*); black boxes indicate standard deviations of the individual experiments, with N = 9 grief (Gf), N = 8 thief (Th), N = 12 granny (Gy), N = 16 reef (Re), N = 6 alpine butterfly (Ab), and N = 6 Zeppelin (Ze) knots. For complex knots with high crossing number, such as the Zeppelin bend, more sophisticated models accounting for material-specific friction forces and three-dimensional contact details need to be developed in the future. Fiber diameter is 0.15 mm. (**C**) Nonetheless, simulations of complex bends with generic friction (*28*) show good shape agreement with tight configurations of bends in nylon ropes (diameter, 20 mm) and reveal the highly nonuniform strain distributions in such knots.

and C). In analogy to the coarse-graining procedure underlying Ising-type spin models, we can associate a unit twist charge $q_i = \pm 1$ with each vertex i in the planar 2-tangle diagram, where the sign of q_i reflects the combined handedness of the torques acting on the two intersecting strands (Fig. 2C). The sum $Wr = \sum_i q_i$, mathematically known as the writhe, represents the total self-torque of a 2-tangle, establishing a concrete link between topology and mechanics.

A key puzzle of physical knot theory (*9*), the empirically observed mechanical difference between the visually similar reef and granny knots (Fig. 3, A and B), may be understood as a consequence of this torque–writhe correspondence in 2-tangles. The underlying mechanism becomes evident by considering a pair of crossings as shown in Fig. 3C. Whereas equally directed torques lead to rolling, opposite torques promote locking and thus stabilize a knot against untying. The overall stability of 2-tangles therefore depends on the self-torque distribution along the fibers, as encoded by the vertex twist charges $q_i = \pm 1$ in an untightened knot diagram (Fig. 3, D to F). The above argument suggests the following topological twist fluctuation energy per site:

$$\tau = \frac{1}{N}\sum_i (q_i - \bar{q})^2 = \tau_0(N) - \frac{2}{N^2}\sum_{i<j} q_i q_j \qquad (1)$$

where N is the crossing number, $\bar{q} = (1/N)\sum_i q_i = Wr/N$ is the average writhe, and $\tau_0 = 1 - 1/N$ can be interpreted as a ground-state energy density (*28*). Equation 1 has the form of a ferromagnetic energy for an Ising-type spin model with long-range interactions, emphasizing the concept of knots as strongly coupled systems.

In addition to twist locking for large values of τ, knots can be stabilized when their internal structure forces fiber segments to slide tangentially against each other. For example, the reef knot and the thief knot both have τ = 1, but because their pulled ends differ, friction makes the reef knot more stable (Fig. 3, D and G). At the coarse-grained level of planar knot diagrams, these friction effects correspond to edge-to-edge interactions dominated by pairs of edges sharing a face and pulled in opposite directions (Fig. 3, D to F). To formalize this notion, each edge around a face F is assigned a weight of +1 or −1 if it winds around F in the anticlockwise or clockwise direction, respectively. Each face then contributes a friction energy given by the net circulation of the edges around the face, C_F, normalized by the total number of edges e_F. This yields the total circulation energy:

$$\Gamma = \sum_F \frac{|C_F|}{e_F} \qquad (2)$$

where the sum is taken over all faces of the knot diagram. The normalization encodes the assumption that every face has the same perimeter in the tight limit, ensuring that each face contributes a maximum of +1 to Γ.

The topological parameters N, τ, and Γ allow us to rationalize the stability of a large class of popular knots used by sailors and climbers (Fig. 3G). These variables are easy to evaluate from knot diagrams (Fig. 3, D to F) and reflect topology-induced forces and torques throughout the knot. As such, the triplet (N, τ, Γ) captures both essential topological and mechanical structure hidden within knots. The (N, τ, Γ) phase diagram explains existing empirical knowledge for simple knots (*2*), as well as predictions of the Kirchhoff model about the relative strength and stability of more complex 2-tangles (Fig. 3G). We verified these predictions independently in experiments by mimicking the prisoner's escape problem (Fig. 4A) with two thin Dyneema fibers made from ultra–high molecular weight polyethylene tied together (*28*). Of the two pulled ends for each knot, one is fixed in the experimental apparatus and the other is perturbed while suspending incrementally higher masses until the knot pulls through. Although the Kirchhoff model cannot account for surface contact details (*30*), the experimental data for the critical loads agree quantitatively with the simulations for simple knots and, more importantly, confirm the predicted qualitative stability differences between various commonly used knots (Fig. 4B). Notably, both theory and experiments indicate that the Zeppelin knot is more secure against untying than the popular alpine butterfly knot (Fig. 4, B and C).

To conclude, the above analysis shows how basic topological counting rules can be used to estimate the relative stability of frequently encountered knots and tangles. From a theoretical perspective, the parallels with long-range coupled spin systems suggest that the statistical mechanics (*4*, *21*) of general knotted structures can be formulated within this framework. Tangled vortices (*12*, *17*) in complex fluids and defect loops in liquid crystals (*15*) may permit similar statistical descriptions through reduction to topological crossing diagrams. In elastic systems, joint experimental and theoretical progress is needed to untangle long-standing puzzles regarding the statistics of knots in DNA (*18*) and proteins (*20*, *21*), where thermal effects induce a finite persistence length, and other macroscopic structures (*8*, *24*). In sailing, climbing, and many other applications, nontopological material parameters and contact geometry (*30*) also play important mechanical roles and must be included in more refined continuum models to quantitatively describe practically relevant knotting phenomena. From a broader conceptual and practical perspective, the above topological mechanics framework seems well suited for designing and exploring new classes of knots with desired behaviors under applied load.

REFERENCES AND NOTES

1. J. C. Turner, P. van de Griend, Eds., *History and Science of Knots*, vol. 11 of *K & E Series on Knots and Everything* (World Scientific, 1996).
2. C. W. Ashley, *The Ashley Book of Knots* (Doubleday Books, 1944).
3. J. B. Trimbos, *Obstet. Gynecol.* **64**, 274–280 (1984).
4. C. C. Adams, *The Knot Book: An Elementary Introduction to the Mathematical Theory of Knots* (American Mathematical Society, 2004).
5. B. Audoly, N. Clauvelin, S. Neukirch, *Phys. Rev. Lett.* **99**, 164301 (2007).
6. M. K. Jawed, P. Dieleman, B. Audoly, P. M. Reis, *Phys. Rev. Lett.* **115**, 118302 (2015).
7. B. F. Bayman, *Am. J. Phys.* **45**, 185–190 (1977).
8. P. B. Warren, R. C. Ball, R. E. Goldstein, *Phys. Rev. Lett.* **120**, 158001 (2018).
9. J. A. Calvo, K. C. Millett, E. J. Rawdon, Eds., *Physical Knots: Knotting, Linking, and Folding Geometric Objects in R^3*, vol. 304 of *Contemporary Mathematics* (American Mathematical Society, 2001).
10. W. Thomson II, *Philos. Mag.* **34**, 15–24 (1867).
11. H. K. Moffatt, R. L. Ricca, "Helicity and the Călugăreanu invariant" in *Knots And Applications*, L. H. Kauffman, Ed. (World Scientific, 1995), pp. 251–269.
12. D. Kleckner, W. T. Irvine, *Nat. Phys.* **9**, 253–258 (2013).
13. M. W. Scheeler, W. M. van Rees, H. Kedia, D. Kleckner, W. T. M. Irvine, *Science* **357**, 487–491 (2017).
14. S. Kuei, A. M. Słowicka, M. L. Ekiel-Jeżewska, E. Wajnryb, H. A. Stone, *New J. Phys.* **17**, 053009 (2015).
15. U. Tkalec, M. Ravnik, S. Čopar, S. Žumer, I. Muševič, *Science* **333**, 62–65 (2011).
16. J. B. Taylor, *Phys. Rev. Lett.* **33**, 1139–1141 (1974).
17. D. Kleckner, L. H. Kauffman, W. T. Irvine, *Nat. Phys.* **12**, 650–655 (2016).
18. R. Stolz *et al.*, *Sci. Rep.* **7**, 12420 (2017).
19. A. R. Klotz, B. W. Soh, P. S. Doyle, *Phys. Rev. Lett.* **120**, 188003 (2018).
20. P. Virnau, L. A. Mirny, M. Kardar, *PLOS Comput. Biol.* **2**, e122 (2006).
21. R. C. Lua, A. Y. Grosberg, *PLOS Comput. Biol.* **2**, e45 (2006).
22. D. Goundaroulis *et al.*, *Polymers* **9**, 444 (2017).
23. R. C. Ball, M. Doi, S. F. Edwards, M. Warner, *Polymer* **22**, 1010–1018 (1981).
24. C. Baek, A. O. Sageman-Furnas, M. K. Jawed, P. M. Reis, *Proc. Natl. Acad. Sci. U.S.A.* **115**, 75–80 (2018).
25. R. D. Kamien, *Eur. Phys. J. B* **1**, 1–4 (1998).
26. J. R. Goldman, L. H. Kauffman, *Adv. Appl. Math.* **18**, 300–332 (1997).
27. M. Kolle *et al.*, *Adv. Mater.* **25**, 2239–2245 (2013).
28. Materials and methods are available as supplementary materials.
29. M. Bergou, M. Wardetzky, S. Robinson, B. Audoly, E. Grinspun, *ACM Trans. Graph.* **27**, 63 (2008).
30. J. H. Maddocks, J. B. Keller, *SIAM J. Appl. Math.* **47**, 1185–1200 (1987).
31. V. P. Patil, Knot simulation code. Zenodo (2019); https://doi.org/10.5281/zenodo.3528928.

ACKNOWLEDGMENTS

J.D. thanks the Isaac Newton Institute for Mathematical Sciences for support and hospitality during the program "The Mathematical Design of New Materials" (supported by EPSRC grant EP/R014604/1) when work on this paper was undertaken. We thank J. Takagi for producing Fig. 4A. **Funding:** This work was supported by an Alfred P. Sloan Research Fellowship (J.D.), a Complex Systems Scholar Award from the James S. McDonnell Foundation (J.D.), the Brigham and Women's Hospital through a Stepping Strong Innovator Award (J.D.S. and M.K.), and the National Science Foundation through the "Designing Materials to Revolutionize and Engineer our Future" program (DMREF-1922321 to J.D.S. and M.K.). **Author contributions:** V.P.P. and J.D. developed theory. V.P.P. performed simulations, for which J.D.S. and M.K. provided data and code for converting strain into perceived knot color. J.D.S. and M.K. designed color-changing fibers and conceived optomechanical experiments. J.D.S. conducted optomechanical experiments and provided the description of the experiments in the supplementary materials. J.D.S. and V.P.P. performed in-lab prisoner's escape experiments. V.P.P. and J.D. wrote the first draft of the paper. All authors discussed and revised the manuscript. **Competing interests:** The authors declare no competing interests. **Data and materials availability:** The code used for numerical simulations is available on Zenodo (*31*). All data are available in the main text or the supplementary materials.

SUPPLEMENTARY MATERIALS

science.sciencemag.org/content/367/6473/71/suppl/DC1
Materials and Methods
Supplementary Text
Figs. S1 to S6
Tables S1 and S2
Movies S1 and S2
References (*32*–*33*)

5 August 2019; accepted 15 November 2019
10.1126/science.aaz0135